Tellus SERIES A DYNAMIC METEOROLOGY AND OCEANOGRAPHY
PUBLISHED BY THE INTERNATIONAL METEOROLOGICAL INSTITUTE IN STOCKHOLM

Applications of point vortex equilibria: blocking events and the stability of the polar vortex

By ANNETTE MÜLLER*, PETER NÉVIR*, LISA SCHIELICKE, MIRJAM HIRT, JOSCHA PUELTZ and ISABELL SONNTAG, *Institute for Meteorology, Freie Universität Berlin, Berlin, Germany*

(Manuscript received 17 July 2015; in final form 20 November 2015)

ABSTRACT

The present study investigates non-linear dynamics of atmospheric flow phenomena on different scales as interactions of vortices. Thereby, we apply the idealised, two-dimensional concept of point vortices considering two important issues in atmospheric dynamics. First, we propose this not widely spread concept in meteorology to explain blocked weather situations using a three-point vortex equilibrium. Here, a steady state is given if the zonal mean flow is identical to the opposed translational velocity of the vortex system. We apply this concept exemplarily to two major blocked events establishing a new pattern recognition technique based on the kinematic vorticity number to determine the circulations and positions of the interacting vortices. By using reanalysis data, we demonstrate that the velocity of the tripole in a westward direction is almost equal to the westerly flow explaining the steady state of blocked events. Second, we introduce a novel idea to transfer a stability analysis of a vortex equilibrium to the stability of the polar vortex concerning its interaction with the quasi-biennial oscillation (QBO). Here, the point vortex system is built as a polygon ring of vortices around a central vortex. On this way we confirm observations that perturbations of the polar vortex during the QBO east phase lead to instability, whereas the polar vortex remains stable in QBO west phases. Thus, by applying point vortex theory to challenging problems in atmospheric dynamics we show an alternative, discrete view of synoptic and planetary scale motion.

Keywords: point vortices, blocked events, polar vortex, Holton–Tan mechanism, kinematic vorticity number, pattern recognition

1. Introduction

Persistent weather situations often have devastating consequences, such as draughts or floods. Examples of these long-lasting weather situations are blocked events in the extratropical regions of the midlatitudes that often last for weeks up to months. In summer 2003, such a blocked weather situation caused the West-European heat wave; simultaneously there was strong precipitation in East Europe. Also the heat wave around Moscow in summer 2010 was caused by a blocked situation. During the same time Pakistan had to struggle against floods. A recent blocked weather situation took place in July 2014, where a blocked high over Norway lead to the warmest July since the beginning of weather recording in 1900 (NMI, 2014).

In general, Rossby theory, which describes successfully propagating waves in a zonal flow, dominates the thinking of large-scale atmospheric motions. A first explanation of blocked events is stationary Rossby waves in a zonal mean flow, which can be ascribed to Yeh (1949). A shortcoming of this global explanation is the missing description of non-periodic, local characteristics of blocked events. Therefore, a modern view on stationary patterns is based on Rossby-wave breaking giving rise to more local, cut-off structures diagnosed by PV-anomalies on isentropic surfaces (Altenhoff et al., 2008). In this context, we propose a physical model based on first principles regarding the large-scale processes as local interactions of several discrete vortices. This approach is reasonable, because the observations show that blocked events are realised by two or three isolated vortices represented by high over low or omega-blocked weather patterns.

A second phenomenon that is usually described by wave mean flow interactions is the break down of the polar vortex

*Corresponding author.
email: annette.mueller@met.fu-berlin.de; peter.nevir@met.fu-berlin.de

Citation: Tellus A 2015, **67**, 29184, http://dx.doi.org/10.3402/tellusa.v67.29184

caused by mid-winter major warmings of the stratosphere. It was discovered by Holton and Tan (1980, 1982) that the dynamics of the northern hemispheric polar vortex are influenced by the equatorial quasi-biennial oscillation (QBO), resulting in a particularly strong polar vortex with negative temperature anomalies during the QBO west phase and a weakened and warmer polar vortex during the QBO east phase. Current research focuses on the divergence of the EP-flux, and therefore vertical propagating Rossby waves. Because the polar vortex is the strongest isolated vortex in the earths' atmosphere, it is reasonable to transfer the problem to the analysis of the stability of point vortex theory.

In this paper, we will consider these two challenging atmospheric issues by the non-linear interaction of isolated vortices. From a theoretical point of view, the classical and simplest way to describe motions on a synoptic and planetary scale is a two-dimensional, barotropic, inviscid and non-divergent model that is mathematically represented by the corresponding vorticity equation; thereby, the property of being divergence-free is realised by the geostrophic wind. The concept that satisfies the required properties of being local and discrete is the classical point vortex theory pioneered by Helmholtz (1858) and Kirchhoff (1876). Surprisingly, there are rather few publications on the application of point vortices to understand large-scale motions in the atmosphere, see for example Charney (1963), Obukhov et al. (1984), Morikawa and Swenson (1971), Friedlander (1975), Egger (1992), DiBattista and Polvani (1998) or Newton (2013).

The central focus of this paper is to demonstrate the diversity of applications to atmospheric flow phenomena under a unified theoretical approach of point vortex theory. In the following section, we will give a short introduction to point vortex theory by explaining the main conserved quantities and equations of motion. In Section 3, we will focus on the equilibrium state for multiple vortices. Data and methods to calculate the circulations will be presented in Section 4. In Section 5, we will give two examples of the applicability of point vortex dynamics to blocked situations. Thereby, we use the concept of three-point vortices building a relative equilibrium. The first example deals with the severe drought over the European part of Russia in 2010; in the second example, we will analyse an omega block over the North Pacific 2011. In Section 6, we will give an example of the applicability of point vortex equilibria to planetary scale and investigate the stability of the polar vortex by multiple point vortex systems. Finally, we summarise our results in Section 8.

2. Point vortex theory

The first investigations on the dynamics of point vortices in the plane were introduced by Helmholtz in 1858. Twenty years later, Kirchhoff presented the general Hamiltonian structure of N point vortices and Gröbli analysed in detail the motion of three-point vortices (Kirchhoff, 1876; Gröbli, 1877). Since then, numerous papers have been published on the motion of point vortices, see for example the works of Novikov (1975), Newton (2013) or Aref (2007). In the following, let v be a solenoidal vector field, that is, $\nabla\cdot\mathbf{v}=0$, and denote $\omega=\nabla\times\mathbf{v}$ the vorticity vector. An important quantity in vortex dynamics is the circulation Γ that is defined by

$$\Gamma=\oint_C \mathbf{v}\cdot d\mathbf{s}=\int_A \omega\cdot\mathbf{n}\,dS, \tag{1}$$

where C is a closed curve on a material plane. Thereby, to achieve the right hand side with area A and normal vector $\mathbf{n}$, Stokes theorem was applied. Moreover, assuming ideal incompressible fluids with conservative forces, Kelvin's circulation theorem states that the circulation Γ around a closed material curve moving with the fluid is constant. To apply point vortex theory to the synoptic and planetary scale, we contract local vorticity fields with the same sign to singular points. During this limiting process, the circulation [eq. (1)] remains constant. This asymptotic transition leads to a physical discretisation of the vorticity field.

In the following, we will give an overview of the basic point vortex equations similar to Müller and Névir (2014). We will denote $\mathrm{x}_i=(x_i\,y_i)^T$ the local coordinates of the i-th point vortex in the plane characterised by their circulation Γ_i, $i=1, 2, \ldots, n$. Further, denote $r_{ij}=((x_i-x_j)^2+(y_i-y_j)^2)^{1/2}$ the relative distance of the i-th and j-th point vortex ($i, j=1, \ldots, n$). Then, the equations of motion derived by Helmholtz (1858) are given by

$$\begin{aligned}\frac{dx_j}{dt}&=-\frac{1}{2\pi}\sum_{\substack{i\neq j\\ i,j=1}}^{N}\frac{\Gamma_i(y_j-y_i)}{r_{ij}^2}\\ \frac{dy_j}{dt}&=+\frac{1}{2\pi}\sum_{\substack{i\neq j\\ i,j=1}}^{N}\frac{\Gamma_i(x_j-x_i)}{r_{ij}^2}\end{aligned} \tag{2}$$

Kirchhoff (1876) established the Hamiltonian representation of these equations of motion as non-linear coupled system of $2N$ ordinary differential equations:

$$\Gamma_i\frac{dx_i}{dt}=\frac{\partial H}{\partial y_i},\qquad \Gamma_i\frac{dy_i}{dt}=-\frac{\partial H}{\partial x_i} \tag{3}$$

with the total energy H of a N-vortex system that is given by

$$H=-\frac{1}{4\pi}\sum_{\substack{i\neq j\\ i,j=1}}^{N}\Gamma_i\Gamma_j\ln(r_{ij}). \tag{4}$$

Furthermore, Kirchhoff has already shown the conservation of the *zonal momentum* P_x, the *meridional momentum*

P_y and the vertical component of the *angular momentum* L_z (Kirchhoff, 1876):

$$P_x(x_i, y_i) = \sum_{i=1}^{N} \Gamma_i y_i \tag{5}$$

$$P_y(x_i, y_i) = -\sum_{i=1}^{N} \Gamma_i x_i \tag{6}$$

$$L_z(x_i, y_i) = -\frac{1}{2} \sum_{i=1}^{N} \Gamma_i (x_i^2 + y_i^2). \tag{7}$$

Moreover, Kelvin's circulation theorem allows us to conclude that the following scalars, the total circulation Γ and the quadratic sum of all circulations, are conserved:

$$\Gamma_{\text{tot}} := \sum_{i=1}^{N} \Gamma_i, \qquad V := \frac{1}{2} \sum_{\substack{i,j=1 \\ i \neq j}}^{N} \Gamma_i \Gamma_j. \tag{8}$$

A composition of P_x, P_y and Γ leads to a further important conserved quantity called the centre of circulation $\mathbf{C}$:

$$\mathbf{C} = \frac{\sum_i^N \Gamma_i \mathbf{x}_i}{\sum_i^N \Gamma_i}. \tag{9}$$

Assuming the total circulation being not equal to zero, point vortices move around their common centre of circulation. Thereby, the orientation of a rotating N-vortex system depends on the sign of the circulation of highest absolute value. But a whole point vortex system can also have zero total circulation. For $\Gamma_{\text{tot}} \to 0$, $\mathbf{C}$ approaches infinity. Therefore, if $\Gamma_{\text{tot}} = 0$, each vortex may rotate, but the geometric central point of the N-vortex system translates. A translating point vortex system with vanishing total circulation will later be applied to describe blocked situations.

There are several concepts to describe point vortex dynamics. We can solve the equations of motion [eq. (2)] based on the local coordinates, or we can describe the motion in terms of the relative distances, such as in Synge (1949), where he introduced tri-linear coordinates or Müller and Névir (2014) who investigated a geometric representation of vortex motion.

2.1. *Atmospheric scales of circulation*

A common approximation of large-scale atmospheric dynamics is to neglect dissipative processes. This approach is used in Rossby-wave theory as well as in vortex dynamics. However, to relate space and time scales of different vortex patterns we follow the principle idea of Kolmogorov (1941) taking dissipation into account.

One of the most important quantities in vortex theory is the circulation that is explicitly given in the point vortex equations [eq. (2)]. In order to analyse the atmospheric scales of circulation, we follow the idea of the dimensional analysis of Kolmogorov (1941). He considered constant dissipation of energy ε leading to a relation between the characteristic time T and the characteristic length L: $T = \varepsilon^{-1/3} L^{2/3}$. This provides a power law of the characteristic circulation Γ in terms of L:

$$\Gamma = \varepsilon^{1/3} L^{4/3}. \tag{10}$$

Motivated by Kolmogorovs idea, we assume constant dissipation of circulation, that is, $\dot{\Gamma} =: \mu = const$. Since the dimension of Γ is given by $L^2 T^{-1}$, we can express the dissipation of circulation in terms of this characteristic quantities: $\mu = L^2 T^{-2}$. Thus, we get the relation of the characteristic time and the characteristic length L:

$$T = \mu^{-1/2} L. \tag{11}$$

In contrast to the assumption of a constant dissipation of energy [eq. (10)], eq. (11) represents a linear relation between T and L. Moreover, $\Gamma = L^2 T^{-1}$ and eq. (11) lead to the linear relationship:

$$\Gamma = \mu^{1/2} L \tag{12}$$

which is illustrated in eq. (1). The dashed line indicates the circulation with respect to the characteristic lengths in terms of the dissipation of energy [$\varepsilon = 5 \cdot 10^{-4}\,\text{m}^2\,\text{s}^{-3}$, Brunt (1939)] and the solid line illustrates the linear relation given in eq. (12) in terms of the dissipation of circulation ($\mu = 264\,\text{m}^2\,\text{s}^{-2}$). This estimation of the dissipation of circulation follows from Schielicke et al. (2015). For the circulations of the omega block, Fig. 1 indicates circulations in the order of 10^7–$10^8\,\text{m}^2\,\text{s}^{-1}$ and larger circulations for the polar vortex in the order of magnitude of

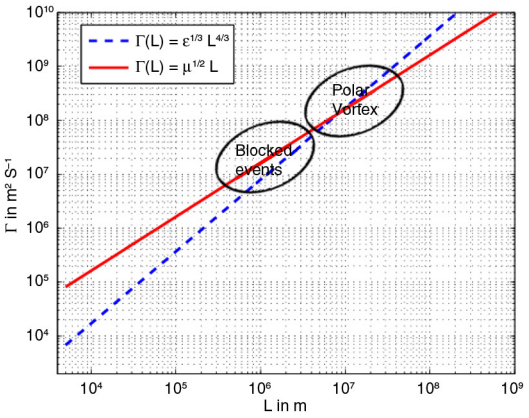

Fig. 1. The order of magnitude of circulations with respect to different lengths scales for the dissipation of energy $\varepsilon = 5 \cdot 10^{-4}\,\text{m}^2\,\text{s}^{-3}$ and the dissipation of circulation $\mu = 264\,\text{m}^2\,\text{s}^{-2}$.

10^8–$10^9\,m^2\,s^{-1}$. We will see that these orders of magnitude coincide with our calculations of the circulations and distances of the real atmospheric vortices.

3. Relative point vortex equilibria

Point vortex motions can be classified into two different kinds of motions. For most initial conditions, the relative distances vary in time, but in special cases they are constant in time. These cases are named relative equilibria. The first investigations of related equilibria took place more than 100 years ago. Mayer (1878) studies equilibrium configurations of the interactions of floating magnets with a strong magnetic field. These configurations turned out to correspond to point vortex equilibria. Since then numerous studies on point vortex equilibria have been followed, see for example Novikov (1975), Aref (1979), Dritschel (1985) or Aref et al. (2012).

In the following, we will apply point vortex equilibria to flow patterns on a synoptic and planetary scale characterised by a low dimensional number of distinguished vortices. On a synoptic scale, dipole and tripole structures can be described as two- or three-point vortex systems. Denote Γ_1 and Γ_2 the circulations of a two vortex system. For $|\Gamma_1| \neq |\Gamma_2|$, the two-point vortex system rotates around its centre of circulation, where each vortex moves along a different circle. In case $\Gamma_1 = \Gamma_2$, both vortices rotate on the same circle. If $\Gamma_1 = -\Gamma_2$, the centre of circulation lies in infinity, and therefore, the two vortex system translates with constant velocity. These two last cases are called relative equilibria and can be applied to atmospherical dipole structures (see Kuhlbrodt and Névir, 2000).

We will extend this idea and discuss omega blocks by three-point vortex equilibria. A first approach to study droughts was given by Obukhov et al. (1984) (in Russian) who realised the idea in terms of climatological geopotential anomalies. The relative equilibrium of three-point vortices occurs either for collinear initial states or for three-point vortices forming an equilateral triangle. In the case of an equilateral triangle and total circulation unequal to zero, the three-vortex system rotates about its centre of circulation with rotation frequency $\omega = (\Gamma_1 + \Gamma_2 + \Gamma_3)/2\pi r^2$, where r is the triangle side (Newton, 2013). In the case of zero total circulation, the centre of circulation lies in infinity. Now let Δ_{123} be an equilateral triangle with the local point vortex coordinates as vertices and equal intervortical distances $r := r_{12} = r_{23} = r_{31}$. Applying eq. (2) leads to the following translation velocity:

$$v = |\mathbf{v}| = \frac{\sqrt{2(\Gamma_3^2 + \Gamma_1^2 + \Gamma_2^2)}}{4\pi r}. \tag{13}$$

For $\Gamma_1 = \Gamma_2$, the system translates along the straight line through vortex 1 and vortex 2. As we have derived in Müller and Névir (2014), varying the circulations leads to the following translation angle:

$$\alpha = \arctan\left(\frac{\Gamma_1 - \Gamma_2}{\sqrt{3}\Gamma_3}\right). \tag{14}$$

In Section 5, we will use the translation velocity [eq. (13)] of a three vortex system to explain the stationarity of blocked weather situations. Omega blocks are characterised by two low-pressure areas south–east and south–west of a high-pressure area (see Fig. 2). Thus, if both lows have equal circulations and are located on the same latitude and if the circulation of the high is twice as large as each low, the total sum of circulation is equal to zero. Therefore, the vortex system translates along the latitude.

In Section 6, we will apply multiple vortex equilibria to study the stability of the polar vortex in the stratosphere. Already in 1883, Thomson analysed the stability of co-rotating vortices on the plane by placing equally spaced vortices with identical circulation along a circle (Thomson, 1883). He proved that these polygonal configurations are stable for $N \leq 6$ vortices. Motivated by the observed potential vorticity structure of the stratospheric polar vortex

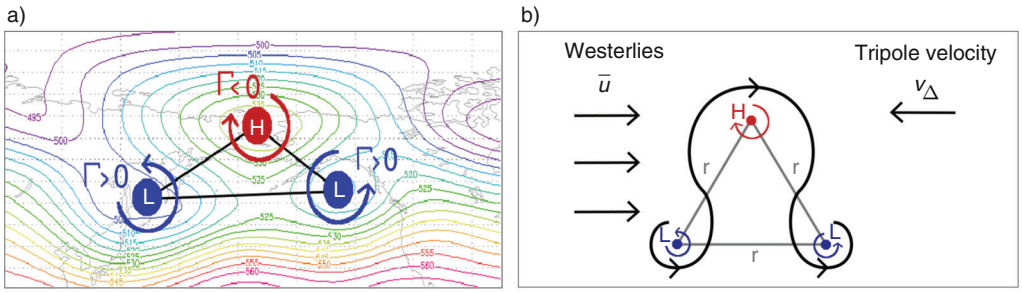

Fig. 2. (a) A three-point vortex equilibrium describes an omega block (geopotential mean over the North Pacific 1–12 March 2011). (b) Such a three-vortex system that represents an omega block translates eastwards, if the total circulation $\Gamma = \Gamma_1 + \Gamma_2 + \Gamma_3$ vanishes. Stationarity can be explained if the translation velocity v_Δ westwards is equal to the velocity of the zonal mean flow $\bar{u}$ eastwards denoted as westerlies in the meteorological context.

Polvani and Dritschel (1993) extended the Thomson's results and studied the stability of a ring of point vortices on the sphere. They have shown that the polygon-rings on the sphere are more unstable than those in the plane. Barry et al. (2012) analysed the relative equilibria of the (N+1) vortex problem with small vortices on a circle of fixed radius around the large vortex which is also fixed. In these configurations, N equally spaced vortices build a polygon with +1 vortex located in the polygon-centre of the polygon ring.

In Section 6, we will show applications of $n=8+1$ point vortex systems to the stratosphere. By applying the theoretical stability condition of Cabral and Schmidt (2000), we propose a novel idea to explain the stability of the polar vortex and its interaction with the east and west phases of the QBO by $n=8+1$ point vortex systems with 8 equally spaced vortices on a polygon and +1 polar vortex.

4. Methods and data

To apply point vortex theory to large-scale atmospheric flow patterns, we discretise the dynamics by contracting the high- and low-pressure areas to points. Furthermore, to use the analytical equations of motion [eq. (2)], we need to determine the circulations and the relative distances of the vortices. If the centres of the vortices are known, the relative distances can be easily measured. But the determination of the circulations Γ is more complicated and we will use both a geometrical and a numerical method to calculate the circulations. Moreover, to apply the method to determine the circulation and also to calculate the basic flow, we use reanalysis data.

4.1. Geometrical method to calculate the circulations

To calculate the circulation Γ_i of a point vortex geometrically, we use a method to estimate the circulation by integrating a loop around the geopotential field of the blocking high/low:

$$\Gamma_i = \frac{g}{f} \sum_k |\delta Z_k| \ \sin(\alpha_k) \tag{15}$$

with the Coriolis parameter f, the gravity acceleration g, the geopotential height Z and the angle α. For a more detailed description, see Kuhlbrodt and Névir (2000).

4.2. Kinematic vorticity number method to calculate the circulations

Following Schielicke et al. (2015), the circulation of a vortex can also be determined numerically. The size of a vortex is estimated with help of the velocity gradient tensor and its invariants which describe the local motion around a point. The velocity gradient tensor $\nabla\mathbf{v}$ in two dimensions is given by

$$\nabla\mathbf{v} = \begin{pmatrix} \partial u/\partial x & \partial u/\partial y \\ \partial v/\partial x & \partial v/\partial y \end{pmatrix}, \tag{16}$$

where u and v are the horizontal wind components in zonal and meridional direction, respectively. The velocity gradient tensor can be decomposed into the sum of a symmetric tensor $\mathbf{S}$ (rate-of-strain tensor) and an antisymmetric tensor $\mathbf{\Omega}$ (vorticity tensor):

$$\nabla\mathbf{v} = \mathbf{S} + \Omega \tag{17}$$

with

$$\mathbf{S} = 1/2(\nabla\mathbf{v} + (\nabla\mathbf{v})^T) \ , \ \Omega = 1/2(\nabla\mathbf{v} - (\nabla\mathbf{v})^T). \tag{18}$$

While the rate-of-strain tensor $\mathbf{S}$ describes the deformation of the flow field composed of expansion, shearing and stretching deformation, the vorticity tensor $\mathbf{\Omega}$ describes the rotation of the flow. A vortex is identified as a connected region of grid points where the local rate of rotation $\|\mathbf{\Omega}\|$ prevails over the local strain rate $\|\mathbf{S}\|$. Truesdell (1953) introduced the kinematic vorticity number W_k as a ratio of the local rate of strain and the local rate of rotation:

$$W_k = \frac{\|\Omega\|}{\|S\|}. \tag{19}$$

In the case of $W_k > 1$, the local rate of rotation exceeds the local strain rate, $W_k = 1$ in the case of a pure shearing motion and $W_k < 1$ if the deformation is larger than the rotation. With the help of W_k, the boundary of a vortex core is defined by $W_k = 1$ around a vorticity extremum. The circulation of the vortex is calculated by the integral [eq (1)].

4.3. Numerical implementation to determine omega blockings in gridded data

In regularly gridded data (mercator projection), the shape of the tripole point vortex configuration is approximated by an isosceles trapezoid which at least includes parts of the polewards located high and of the two equatorwards located low-pressure systems. The parallel sides of the trapezoid are aligned with two latitudes with the smaller side located polewards. The aim of this pattern recognition method following Schielicke et al. (2015) is to minimise the absolute value of the total circulation $|\Gamma|$. The circulations of the local coordinates of the centres of circulations and the intervortical distances are derived systematically by the following steps:

A trapezoid is fixed to the lat–lon grid such that the vertical centreline of the trapezoid coincides with the

approximated centre of the high-pressure system and its West–East (width)/North–South (height) extent includes (at least most) the high-pressure area as well as parts of the two lows. See Table 1 for more details on the initial configuration of the trapezoids for two real cases.

We will use an ensemble of 45 trapezoid shapes derived by moving the southern baseline of the trapezoid by $\pm 10^{\circ}$ latitude in 2.5° steps and by moving the position of the northern line equatorwards by four steps a 2.5° latitude (summarised in Table 1).

At each time step, the total circulation and the centre of positive and negative circulations associated with the three vortices inside the trapezoids are determined under the following conditions: Only positive circulations located south of the high-pressure centroid and west (east) of the trapezoid centreline contribute to the southwesterly (southeasterly) low; only negative circulations polewards of the low-pressure centroids contribute to the high (see Fig. 3).

For every time step the minimum absolute value of the total circulation, the centre of circulation, the trapezoid configuration, the translation velocity and the relative distances between the circulation centres are determined. Thereby, the local coordinates of the highs and lows are determined by calculating the centres of circulation [eq. (9)] of each high and low-pressure region. An example is given in Fig. 4 where the local coordinates of the centres of the high- and low-pressure systems are indicated by the red/blue circles.

Finally, averaged values of the variables derived in eq. (4) are calculated for the whole blocked period. Moreover, the North–South extent of the averaged trapezoid configuration is used to calculate the mean global wind speed averaged over the same latitudes and period.

4.4. *Reanalysis data*

For the analysis of blocked weather events in summer (June–August) 2010 and March 2011, the horizontal wind field (u, v) and the geopotential height on the 500 hPa level from the NCEP/DOE Reanalysis 2 (R2) Project was used (NCEP, 2000; Kanamitsu et al., 2002). The data is available on a regular 2.5×2.5 degrees grid with a temporal resolution of 6 hours. In order to respect the differing perimeter of the latitudes on the sphere, we weigh the velocity of the zonal mean flow in terms of its latitude, that is, for the zonal mean flow u on the latitude φ_i with radius $R_i = R \cdot \cos(\varphi_i)$ and the earth radius R the weight is given by $(\Sigma_i u(\varphi_i) \cdot R_i) \cdot (\Sigma_i R_i)^{-1}$.

For the numerical investigation of the stability of the polar vortex, NCEP/NCAR reanalysis data also was used, that is, the geopotential height of the December, January, February (DJF) mean 1979–2012 in 30 hPa. For the outer point vortices, the annual mean of the relative vorticity 1997 and 2005 in 30 hPa was built using ERA-Interim reanalysis data (ERA, 2009; Dee et al., 2011) using a 0.7×0.7 degrees grid and a temporal resolution of 6 hours.

5. Application on a synoptic scale: blocked events

In this section, we will give two examples of the applicability of point vortex theory to omega blocks. During blocked events, the basic flow is usually divided into different branches caused by a low number of isolated and persistent vortices. This large-scale feature of the atmospheric flow field was already recognised by Garriott (1904). In 1947, Namias (1947) mentioned that blocked situations are associated with a retardation in the zonal circulation. Yeh (1949) explained blocking situations by the dispersion of an initial solitary wave. One year later, Rex (1950a, 1950b, 1951) characterised in detail different blocked situations: the zonal basic flow should be divided into two branches at which each of the branches needs to transport mass. Moreover, following his definition, the extent of these branches must be at least 45 degrees of longitude and should remain blocked for at least 6–10 days. Usually, during blocked situations a very strong high-pressure area appears.

Bluestein characterises three kinds of blocks (Bluestein, 1992): The simplest blocked event consists of a high-pressure area, and another blocked event is described by a high-pressure area north of a low-pressure area (high over low). A further arrangement consists of a high-pressure area and two low-pressure areas located south–west and south–east. The last weather situation is called omega block and illustrated in Figs. 2 and 4. High temperatures and droughts

Table 1. Initial and final (averaged) configurations of the trapezoids for the omega blocks over Russia in summer 2010 and over the North Pacific in March 2011

	Russia/Europe (Summer 2010)	North Pacific (March 2011)
Points of initial trapezoid	(10 ° E, 80 ° N) (80 ° E, 80 ° N)	(160 ° E, 85 ° N) (220 ° E, 85 ° N)
	(10 ° W, 35 ° N) (100 ° E, 35 ° N)	(140 ° E, 45 ° N) (240 ° E, 45 ° N)
Adjustment of northern line	80 ° N → 70 ° N by 2.5 °	85 ° N → 75 ° N by 2.5 °
Adjustment of southern basis	25 ° N → 45 ° N by 2.5 °	35 ° N → 55 ° N by 2.5 °
Final averaged height	32.5 ° N–75 ° N	46.9 ° N–80 ° N

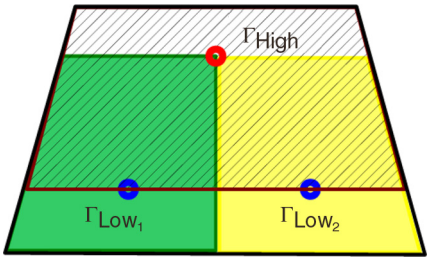

Fig. 3. Trapezoid approximating the region of the omega block. In the green area, the total cyclonic circulation Γ_{Low_1} is calculated, and in the yellow area, the total cyclonic circulation Γ_{Low_2} is determined. The total anticyclonic circulation Γ_{High} is calculated in the striped area.

can be caused by those persistent high-pressure areas that can be stationary for several days or even for months. Moreover, the persistence of the low-pressure areas can lead to heavy rainfalls and floods.

However, the first application to describe stationary, blocked weather situations by three-point vortices, was established by Obukhov et al. (1984). Since then, numerous works on blocks have followed, see for example Bluestein (1992), Pelly and Hoskins (2003) or Bott (2012). After Névir (1998) showed the equivalence of continuous vorticity dynamics and point vortex dynamics via a group theoretical approach, Kuhlbrodt and Névir (2000) applied blocked dipole structures to point vortex motion.

We will discuss analytically stationary solutions of a three-point vortex system. The general applicability of two-dimensional point vortex theory to blocked events is indicated in Fig. 5, where the analytical translation velocity [eq. (13)] of a three-point vortex equilibrium with respect to its intervortical distances is shown. Thereby, each curve represents a three-point vortex system. We chose circulations that are typical on a synoptic scale and that sum up to zero. A main result of our approach is that the point vortex velocity of 5–10 m/s on the typical synoptic scale of 2000–3500 km coincides with the characteristic velocity of atmospheric basic flow. This result leads to a natural explanation of the whole omega block consisting of the three vortices regarding the orientation. The tripole moves eastwards with velocity v_Δ, and the remaining interaction of vortices is parameterised as zonal mean flow leading to the westwards velocity $\bar{u}$. Since both velocities coincide with respect to the magnitude, that is:

$$v_\Delta = -\bar{u}, \tag{20}$$

the stationarity of blocked events can be explained (see Fig. 2b). Because the point vortex constellation should be a relative equilibrium, the total circulation of an ideal blocked event should vanish and therefore it should satisfy

$$\Gamma_{\mathrm{Low}_1} + \Gamma_{\mathrm{Low}_2} = -\Gamma_{\mathrm{High}}. \tag{21}$$

If the local coordinates of the two lows, Γ_{Low_1} and Γ_{Low_2}, are lying on the same latitude, the whole three vortex system translates along this latitude with velocity [eq. (13)]. We do not explain the formation of blocked events, such as Rossby waves do, but we explain the stationarity by considering the local character, whereas wave theory is based on global features.

To include the β-effect, the earth rotation has to be added. Therefore, from an inertial-system perspective the absolute vorticity should be used leading to an absolute circulation [according to eq. (1)] and to modifications of the equations of motion [eq. (2)] considering the absolute point vortex velocity. Moreover, we have to add the effect

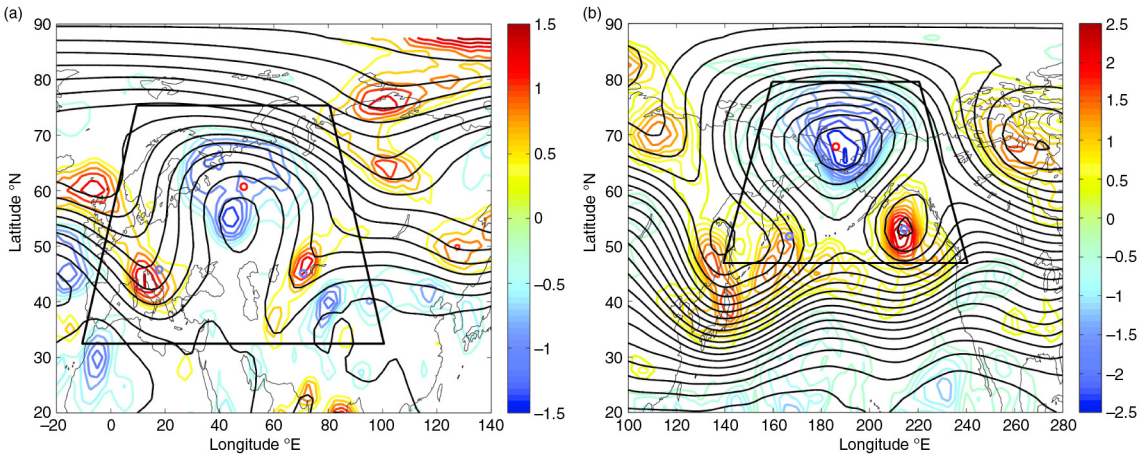

Fig. 4. Temporal averages [(a) 24 July 2010, 00 UTC to 7 August 2010, 18 UTC and (b) 1 March 2011, 00 UTC to 11 March 2011, 12 UTC] of geopotential height (black contours) and relative vorticity (in $10^{-5}\,\mathrm{s}^{-1}$, coloured contours). The vorticity is shown in the field of kinematic vorticity number $W_k > 1$. The trapezoids encircle the area of zero total circulation, and the blue and red circles mark centres of the low- and high-pressure areas, respectively. Note the different ranges of vorticity in the plots.

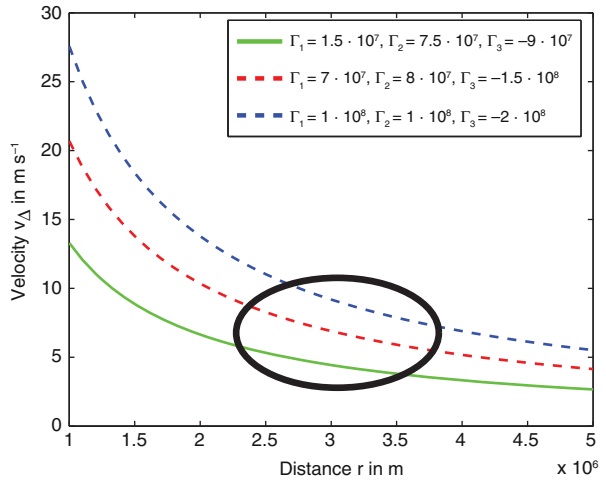

Fig. 5. Translational velocity of a three-point vortex system as a function of the intervortical distances r for three different vortex configurations with vanishing total circulation is shown. For typical distances on a synoptic scale of 2500–3500 km, the absolute value of the analytical translation velocity of 5–10 ms^{-1} of a three-point vortex equilibrium coincides with the typical basic flow velocity.

of the earth rotation to the velocity of the basic flow. By applying eq. (20), both terms considering the effects due to earth rotation would cancel out. Therefore, in the following examples we calculate circulations and the velocities in terms of the relative frame of reference.

5.1. *Example 1: Omega block over Russia 2010*

We will examine the blocked situation in summer 2010, where the blocked high caused a heat wave in the European part of Russia and surrounding countries. During this summer, low precipitation, low wind velocities and fatal forest fires were observed. In Moscow, more than 30 degrees Celsius was measured on more than 40 days; even on 15 days the temperature exceeded 35 degrees Celsius (Friedrich and Bissolini, 2011). Even though 2010 was one of the warmest years since weather recording, large parts of West and Central Europe were colder than the average, which could be ascribed to the two stationary low-pressure areas.

During the time period 18 June 2010–23 July 2010, we recognised a blocked dipole structure followed by an omega block from 24 July 2010 to 07 August 2010. Even though the dipole structure can also be explained by a (two) point vortex equilibrium, we will concentrate on the omega block and explain the persistent structure by point vortex theory.

Thereby, to determine the circulations we first search for the trapezoid-area of zero circulation as we described in Section 4.1. The vertices of the initial trapezoid and the enlargement of the trapezoid boundary are summarised in Table 1. Figure 4a shows the determined final configuration. To identify the low-pressure systems Γ_{Low_1} and Γ_{Low_2}, we use the lower part of the trapezoid, that is, the area south of 60° N. And for the determination of the high-pressure vortex we consider the area north of 45° N.

Table 2. Values of the circulation of the tripole and the locations of the centres over Russia and Europe in summer 2010 and over the North Pacific in March 2011

	Russia/Europe (2010)		North Pacific (2011)	
	Circulation in $m^2 s^{-1}$	Location (°N; °E)	Circulation in $m^2 s^{-1}$	Location (°N; °E)
$\Gamma\mathrm{Low}_1$	$7.543.10^7$	(45.8; 17.7)	$7.090.10^7$	(51.7; 166.7)
$\Gamma\mathrm{Low}_2$	$5.424.10^7$	(45.1; 70.9)	$8.322.10^7$	(53.0; 214.3)
$\Gamma\mathrm{High}_1$	$-1.306.10^8$	(60.7; 48.9)	$-1.546.10^8$	(67.8; 186.0)

The values and local coordinates of the finally determined circulations are summarised in Table 2. These values add up to the total circulation $\Gamma = -0.009 \cdot 10^8\, m^2\, s^{-1}$, which is only 0.71% of Γ_{High}. Thus, the total circulation is still small enough to apply formula (13). The averaged triangle side lengths which are the intervortical distances are given by $\bar{r} = 2910$ km. Applying formula (13) leads to the analytical solution of the tripole translation:

$$v_\Delta = -(6.3 \pm 2)\frac{m}{s}, \tag{22}$$

where the error tolerance is estimated by the calculated minima/maxima intervortical distances of the system. In the same time period, the zonal mean flow averaged in the area 32.5° N–75°N [1] is given by

$$\bar{u} = (6.5 \pm 1)\frac{m}{s}. \tag{23}$$

The sum of the mean flow and the analytical dipole velocity vanishes which explains the stationarity of the tripole.

5.2. *Example 2: Omega block over North Pacific 2011*

As a second example, we will analyse an omega block during the time period 1–12 March 2011 that is shown in Fig. 4b. The circulations are again determined by the numerical method and its values and local coordinates are summarised in Table 2. Here, the circulations of the two lows and the high sum up to $\Gamma = -0.005\, 10^8\, m^2\, s^{-1}$, which is 0.32% of the value of Γ_{High}. The averaged intervortical distance, that is, the side length of the equilateral triangle,

[1] The error tolerance of the basic flow results from the calculation of the maxima/minima mean wind speeds.

is $\bar{r} = 2490\,\text{km}$. Applying formula (13) and including the error estimation provides the tripole velocity:

$$v_\Delta = -(8.8 \pm 2)\frac{\text{m}}{\text{s}}. \tag{24}$$

On the other hand, the mean flow (45° N–80° N) is given by

$$\bar{u} = (8.3 \pm 1)\frac{\text{m}}{\text{s}}. \tag{25}$$

Again, the sum of the flow velocity and the analytically determined point vortex velocity vanishes explaining the stationarity of the block.

5.3. *Modes of disturbed equilibria*

In principle, it is necessary to consider deviations of the perfect equilibrium tripole with vanishing total circulation and equal side lengths, because often we do not observe perfect omega blocks. First, we disturb the equilateral triangle in terms of its side lengths by shifting one vertex by ε. This does not influence the circulations; that is, the centre of circulation still lies in infinity. Therefore, the three vortex system still translates. But in the case of perturbations of the local coordinate, the three vortices do not build a perfect equiangular triangle anymore; therefore, the trajectories of the vortices are given by cycloids with small amplitudes, which is simplified illustrated in Fig. 6. Here, the translational motion is superimposed by an additional pulsating mode. For $\varepsilon \to 0$, these amplitudes approach zero; that is, the cycloid approaches a straight line. Moreover, the translation angle [eq. (14)] is affected by the perturbation ε. Both effects, the pulsating mode and the varying angle only rarely effect the tripole velocity and therefore do not spoil the overall explanations of the persistence of blocked situations.

Second, we disturb the circulation. Thus, the centre of circulation does not lie in infinity anymore. But for a small perturbation the centre of circulation still lies far away from the three-point vortex system and therefore, the vortices move along a large circle, which locally can be assumed as linear translation.

We can summarise that small variations of both, the local coordinates and the circulations do not affect the applicability of point vortex theory to atmospheric blocked events.

6. Application on planetary scale: the stability of the polar vortex

So far, we adapted relative equilibria of point vortex constellations to a synoptic phenomenon. In addition, we apply a stability analysis of relative point vortex equilibria to stratospheric dynamics regarding larger scale, planetary patterns.

One main aspect of point vortex dynamics is the investigation of the stability of relative equilibria. Already in 1883, Thomson investigated stability studies on multiple, equally spaced point vortices on a circle (Thomson, 1883), followed by many other works in this field, see for example Campbell and Ziff (1978), Cabral and Schmidt (2000), or Aref et al. (2012). Charney (1963) extended those configurations of 7, 8 and 16 vortices to atmospheric motion. Based on these works, we introduce a novel idea to transfer a stability analysis of a vortex equilibrium to the stability of the polar vortex concerning its interaction with a simple model of the QBO. In this context, we propose a conceptional explanation of the Holton–Tan mechanism based on discrete, low-order vortex dynamics.

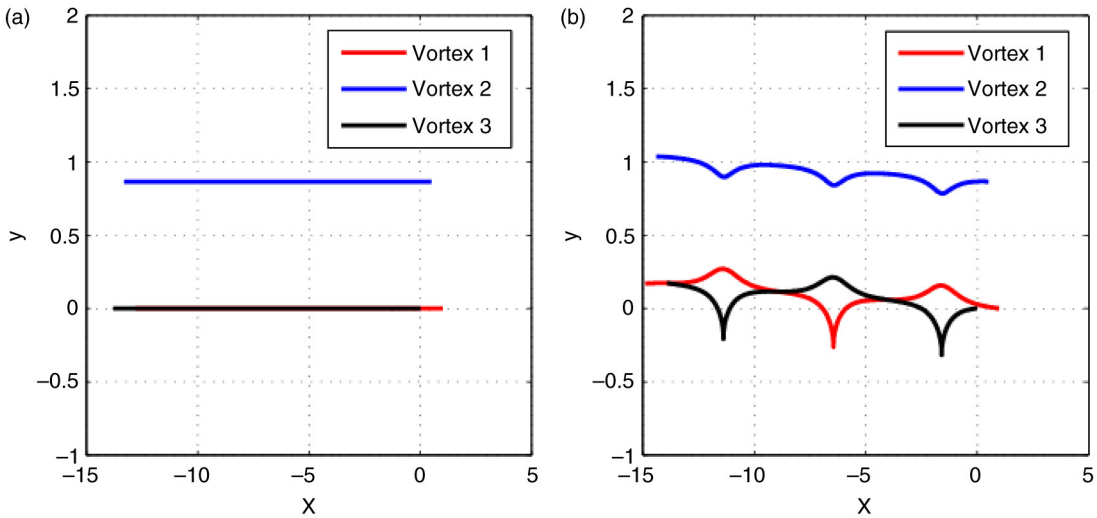

Fig. 6. (a) The equilibrium state for the initial states $\mathbf{x}_1 = (1,0)$, $\mathbf{x}_2 = (0.5, \sqrt{.75})$, $\mathbf{x}_3 = (0,0)$ and $\Gamma_1 = 1$, $\Gamma_2 = -2$, $\Gamma_3 = 1$, which builds an equilateral triangle where total sum of circulations equals zero. (b) Small perturbations of x_3 lead to cycloid motions.

Stratospheric dynamics are mainly determined by the polar vortex, which denotes a major low-pressure system in the polar stratosphere on both hemispheres during wintertime, and the QBO, an equatorial, zonal wind pattern, which changes its direction approximately every 2 yr (see, e.g., Baldwin et al., 2001). In Fig. 7, we show this zonal oscillation in terms of the wind as a time series in the equatorial region in 0–20° N in 30 hPa. Moreover, because of our approach of vortex dynamics, we also illustrate the corresponding mean vorticity. Due to horizontal shearing of the wind, the vorticity oscilates nearly in phase with the zonal wind, even though deviations can be diagnosed. The westerly winds are related to cyclonic vorticity, while the easterly winds correspond to anticyclonic vorticity.

It was first discovered by Holton and Tan (1980, 1982) that the dynamics of the northern hemispheric polar vortex are influenced by the equatorial QBO, resulting in a particularly strong polar vortex with negative temperature anomalies during the QBO west phase and a weakened and warmer polar vortex during the QBO east phase. Approaches to explain the mechanisms of the Holton–Tan effect have been developed, but they are still not well understood (Anstey and Shepherd, 2014; Watson and Gray, 2014). Here we tackle this problem by analysing the stability of point vortex equilibria.

6.1. *Stratospheric configuration of the point vortex model*

6.1.1. Conceptual model. The novel idea in this paper is to analyse the interaction of the polar vortex and the QBO by a low-order, non-linear point vortex model. Following Lim et al. (2001), less concentrated regions of vorticity can be approximated by large numbers of point vortices. Therefore, we parameterise the vorticity distribution of the QBO as a belt of identical point vortices on a regular polygon in the plane with a central, cyclonic point vortex representing the polar vortex. To simulate the QBO west phase, we take cyclonic point vortices whereas the QBO-east phase is represented by anticyclonic point vortices.

Even though the above explained configuration, often called $N+1$ configuration, is a relative equilibrium, it is not necessarily stable. Depending on the number of vortices and their circulations this equilibrium configuration can become unstable. In this case, small perturbations are growing leading to a complete different configuration, while a stable equilibrium will hardly be affected by perturbations. To examine the stability for the $N+1$ relative equilibrium, we consider the criterion of Cabral and Schmidt (2000) for the Lyapunov stability:

$$\begin{aligned} \frac{N^2-8N+8}{16} < \frac{\Gamma_c}{\Gamma_i} < \frac{(N-1)^2}{4} \quad &\text{for N even} \\ \frac{N^2-8N+7}{16} < \frac{\Gamma_c}{\Gamma_i} < \frac{(N-1)^2}{4} \quad &\text{for N odd,} \end{aligned} \tag{26}$$

where Γ_c denotes the vortex lying in the centre and Γ_i is the vortex circulation of the i-th vortex on the polygon ($i=1, \ldots, N$). This criterion was proven for the unit circle and corresponding circulations. The adaption of the analysis to atmospheric scales in terms of the circulation and lengths scales can be realised with the linear relationship between the two parameters derived in eq. (12). As an example for the investigation of vortex equilibria on planetary scale, we will adjust a $8+1$ constellation to stratospheric scales. Subsequently, we use both numerical simulations and this theoretical stability criterion to analyse the point vortex model and its applicability to stratospheric dynamics.

6.1.2. Scaling of the point vortex model. The magnitude of the intervortical distances and the circulation of the point vortices are adapted to atmospheric scales. To determine the circulation of the polar vortex, represented by the central point vortex, the geometrical method [eq. (15)] is used, resulting in an estimated circulation of

$$\Gamma_c = 6 \cdot 10^8 \, m^2 \, s^{-1}. \tag{27}$$

To represent the QBO and its interaction with the polar vortex via point vortex dynamics, we approximate the

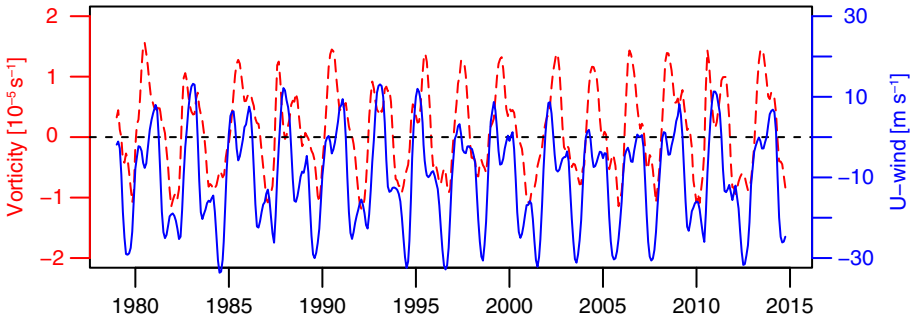

Fig. 7. The quasi-biennial oscillation. The dashed line represents the mean vorticity, and the solid line represents the zonal wind. The data is averaged over 0–20 ° N in 30 hPa.

continuous vorticity distribution by discrete point vortices. Thereby, the total circulation of the outer vortices on the polygon, defined as Γ_{QBO}, is estimated by averaging the relative vorticity ζ in 30 hPa over an equatorial area between 0° N and 20° N:

$$\Gamma_{QBO} := \sum_{i=1}^{8} \Gamma_i \approx \bar{\zeta} \cdot A. \tag{28}$$

In this approximation of the circulation, A is the lateral surface of the spherical segment with respect to the earth's radius. A time series of the vorticity and the resulting circulation for each single QBO phase and the mean for the east and west phases is presented in Fig. 8. For the simulations, the total circulation of the outer vortices is approximated to

$$\Gamma_{QBO} = \pm 5.6 \cdot 10^8 \, m^2 \, s^{-1} \tag{29}$$

with $\Gamma_i = \pm 0.7 \cdot 10^8 \, m^2 \, s^{-1}$ ($i = 1, \ldots, 8$). The sign depends on the phase of the QB0, where positive, cyclonic circulations represent the west phase and negative circulations represent the east phase. In Fig. 8, the value of Γ_{QBO} is marked by the dotted lines and lies within the first standard deviation. The area of 0–20° N has been selected, because the oscillation of the vorticity seems to be strongest in this area.

For our planar point vortex model, we choose as distance between the polar vortex and the vortex polygon 10 000 km approximated as a quarter of the circumference of the earth. To analyse the 8 + 1 point vortex system numerically, the differential equations of motion [eq. (2)] was solved using the Runge-Kutta method of order four.

6.2. *Results of the stability analysis of the polar vortex*

6.2.1. Numerical simulation. To analyse the stability of the adjusted 8 + 1 configurations, we consider two different modes of perturbation. The first perturbation is realised by slightly displacing the central point vortex from the centre. As example, we consider a displacement of 250 km. Compared to the radius of the polygon of 10 000 km, this displacement is hardly visually noticeable. A second type of perturbation is provoked by representing the elliptic extent of the polar vortex by adding a further point vortex near the circulation centre. Thereby, the two vortices are shifted 1500 km and −1200 km in the y-direction from the origin. The circulation of the polar vortex is equally split such that both vortices have the circulation of $3 \cdot 10^8 \, m^2 \, s^{-1}$.

For both phases of the QBO and both types of perturbations, the disturbed initial vortex system and the resulting trajectories after an integration time of 180 days are shown in Fig. 9. Independent of the mode of perturbation, during the west phase of the QBO with cyclonic outer point vortices the relative equilibrium is only slightly disrupted. In this case, Fig. 9 shows a central point vortex and a uniform, stable motion of the outer vortices on a circle for the whole period. In contrast, during east phase with anticyclonic, outer point vortices, the polar vortex is definite unstable. The outer point vortices leave their circular path after a while also. The second example might be even more realistic because in our simulations the split polar vortex rotates as a cycloid around the centre of circulation which reflects the wobbling motion of the polar vortex.

If we do not disturb the relative equilibrium during east phase, we observe the instability of the relative equilibrium after a five-time longer time period. These numerical results of the different phases will be confirmed by the theoretical stability analysis in the next section.

6.2.2. Theoretical stability analysis. The theoretical conditions of Lyapunov stability after Cabral and Schmidt (2000) given in eq. (26) are adapted for the characteristic scales in the stratosphere are illustrated in Fig. 10. The total circulation of the outer vortices Γ_{QBO} given by eq. (29) is

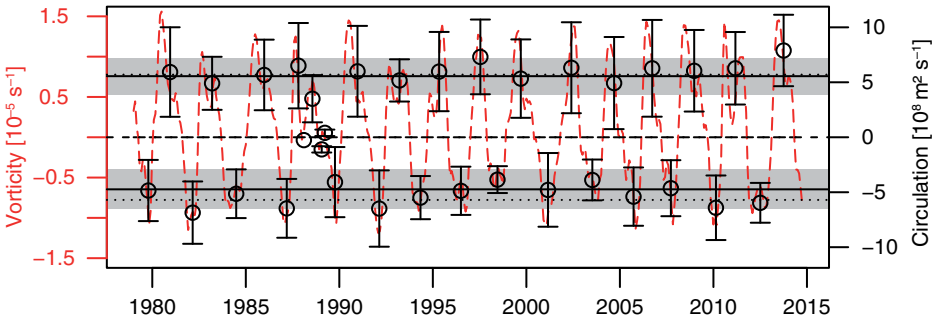

Fig. 8. The dashed line presents the vorticity, averaged over 0–20 ° *N*. The circles indicate the calculated circulation during a single QBO phase (defined by the sign of the vorticity) and the corresponding bars the first standard deviation. The two solid, horizontal lines are the resulting mean circulation for the West and East phase of the QBO respectively. Their standard deviation is marked by the grey-shaded area. The used circulation $\Sigma_i^N \Gamma_i = \pm 5.6 \cdot 10^8 \, m^2 \, s^{-1}$, displayed by the two dotted lines, lies within the first standard deviation.

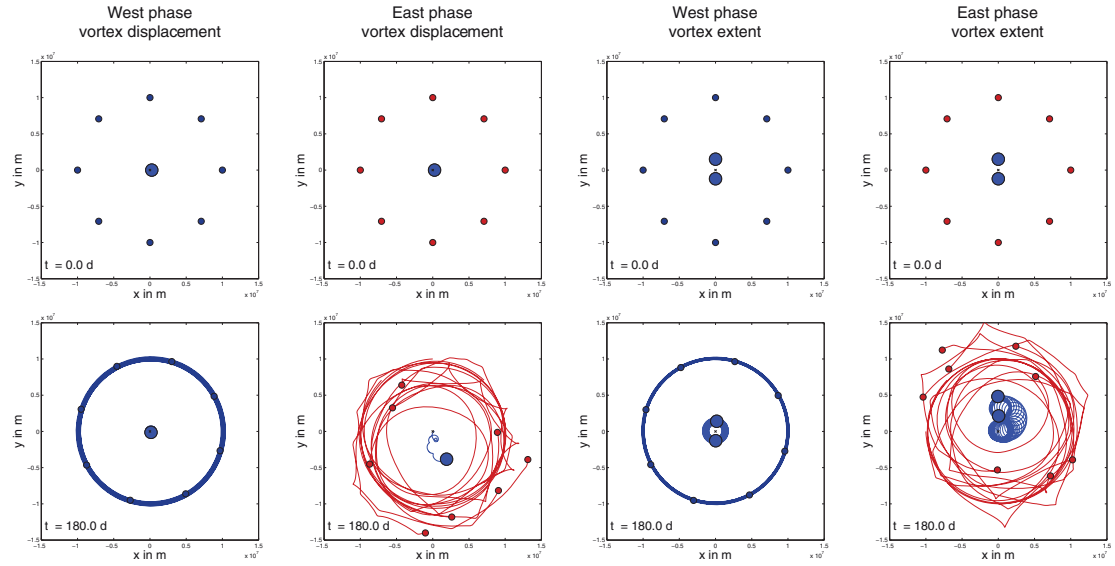

Fig. 9. The perturbed initial states (first row) and the resulting trajectories (second row) are shown for the QBO west phase with cyclonic, outer point vortices (first and third column, coloured blue) and the QBO east phase with anticyclonic, outer point vortices (second and forth column, coloured red). The first and second columns contain the displacement of the central vortex and the third and fourth columns the additional point vortex.

assumed to be constant. Furthermore, the circulation of each outer vortex depends on their total number N and is given by $\Gamma_i = N^{-1}\Gamma_{\mathrm{QBO}}$. Therefore, by increasing the number of point vortices N, the circulation of each outer vortex decreases. Fig. 10 shows that stable configurations for the west phase of the QBO are possible for a certain range of the ratio Γ_c/Γ_i with respect to N. The blue and red lines show our estimated circulations indicating the west and east phase. For the west phase, there is a range of stability depending on the number of outer vortices which is given by $6 < N < 27$. In contrast, Fig. 10 indicates that the red line and all other east phase constellations are located in the unstable region.

Thus, at first we have shown that the theoretical stability results coincide with the numerical simulations. Moreover, these stable and unstable point vortex configurations for the QBO west and east phases can be interpreted as potentially stable and unstable phases in terms of reasonable perturbations in stratospheric dynamics. As a consequence, this might also lead to an explanation of the varying strength of the polar vortex according to the Holton–Tan effect. Stable configurations with cyclonic outer point vortices correspond to the strong and cold polar vortex during the west phase of the QBO and unstable configurations with anticyclonic outer point vortices are in accordance with the weak and warm polar vortex during the east phase of the QBO.

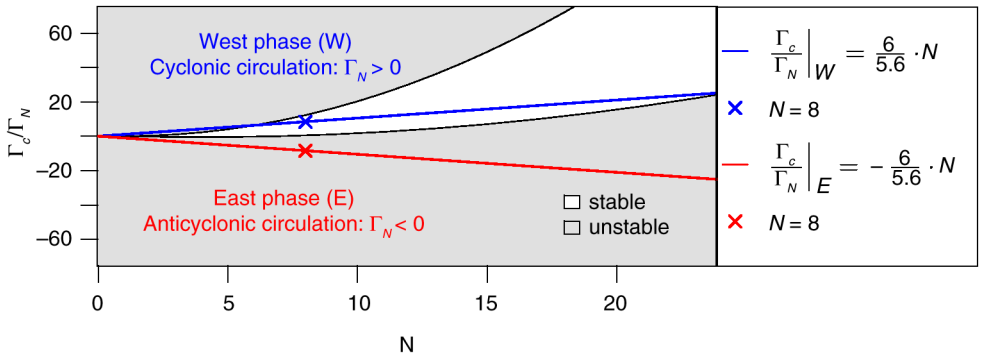

Fig. 10. Stability diagram based on the stability criterion of Cabral and Schmidt (2000) given in eq. (26). The two lines represent the approximate scale of the stratospheric circulations. The vortex states for the west phase (blue line) are stable in a large range, whereas no stable configurations can be found for the east phase (red line). Here, $\Gamma_N = \Gamma_{\mathrm{QBO}} N^{-1}$ denotes the circulation of each outer vortex with $\Gamma_{\mathrm{QBO}} = 5.6 \cdot 10^8\,\mathrm{m^2\,s^{-1}}$, and $\Gamma_c = 6 \cdot 10^8\,\mathrm{m^2\,s^{-1}}$ represents the polar vortex.

7. Concluding remarks

In this work, we have shown the applicability of point vortex theory for a better understanding of phenomena on a synoptic as well as on a planetary scale. A basic conserved quantity under adiabatic, inviscid conditions on material, two-dimensional surfaces is the circulation which is a widely used concept to describe atmospheric motions in meteorology and climatology and which even constitutes the equations of point vortex motion derived from first principles. By assuming constant dissipation of circulation, we showed a linear relation of the characteristic circulation and characteristic lengths in synoptic and planetary scale.

On a synoptic scale, we have given examples for the explanation of blocked weather situations by three-point vortex equilibria. Since the point vortex velocity of a three-vortex equilibrium and the mean zonal wind derived from reanalysis data coincide with respect to their absolute values, the stationarity of blocked situations are explained. Evaluating omega blocks over the European part of Russia and over the North Pacific affirms the possibility to explain the stationarity of blocked events by this low-order point vortex model.

On a planetary scale, we have analysed the interaction between the equatorial stratosphere and the polar vortex by numerical simulations of $8+1$ point vortex equilibria. Concerning the influence of reasonable perturbations, we confirm instability of QBO east phase and stability of QBO west phase during north hemispheric winter period. This is also consistent with the theoretical stability analysis of Cabral and Schmidt (2000). Thereby, we propose a dynamical explanation of the observed Holton–Tan effect during winter period by point vortex theory. The central focus in this novel approach in terms of vortex interactions is the stability analysis of the east and west phases. Further investigations to combine this stability analysis with the more classical wave mean flow approach concerning different types of perturbations are desirable.

We have applied a simple, conceptional model requiring less computational effort to explain two challenging problems in atmospheric dynamics. By demonstrating the applicability of point vortex theory to different atmospheric scales, we underline the diversity of applicability of the classical point vortex model.

8. Acknowledgements

We would like to acknowledge the Helmholtz graduate research school GeoSim for founding this project.

References

Altenhoff, A. M., Martius, O., Croci-Maspoli, M., Schwierz, C. and Davies, H. C. 2008. Linkage of atmospheric blocks and synoptic-scale Rossby waves: a climatological analysis. *Tellus A*. **60**(5), 1053–1063.

Anstey, J. A. and Shepherd, T. G. 2014. High-latitude influence of the quasi-biennial oscillation. *Q. J. Roy. Meteorol. Soc.* **140**(678), 1–21.

Aref, H. 1979. Motion of three vortices. *Phys. Fluids*. **22**(3), 393–400.

Aref, H. 2007. Point vortex dynamics: a classical mathematics playground. *J. Math. Phys*. **48**(6), 065401.

Aref, H., Beelen, P. and Brøns, M. 2012. Bilinear relative equilibria of identical point vortices. *J. Nonlin. Sci*. **22**(5), 849–885.

Baldwin, M. P., Gray, L. J., Dunkerton, T. J., Hamilton, K., Haynes, P. H. and co-authors. 2001. The quasi-biennial oscillation. *Rev. Geophys*. **39**(2), 179–229.

Barry, A. M., Hall, G. R. and Wayne, C. E. 2012. Relative equilibria of the $(1+n)$-vortex problem. *J. Nonlin. Sci*. **22**(1), 63–83.

Bluestein, H. B. 1992. *Synoptic–Dynamic Meteorology in Midlatitudes: Observations and Theory of Weather Systems, Volume 2*. Taylor & Francis, Oxford University Press, Oxford, New York.

Bott, A. 2012. *Synoptische Meteorologie: Methoden der Wetteranalyse und-prognose*. Springer-Verlag, London, New York.

Brunt, D. 1939. *Physical and Dynamical Meteorology*. Cambridge University Press, New York.

Cabral, H. E. and Schmidt, D. S. 2000. Stability of relative equilibria in the problem of n+ 1 vortices. *SIAM J. Math. Anal*. **31**(2), 231–250.

Campbell, L. J. and Ziff, R. 1978. *Catalog of Two-Dimensional Vortex Patterns*. Technical Report, Los Alamos Scientific Laboratory, Alamos, NM.

Charney, J. G. 1963. Numerical experiments in atmospheric hydrodynamics. In Experimental Arithmetic, High Speed Computing and Mathematics. *Proc. Symp. Appl. Math*. **15**, 289–310.

Dee, D. P., Uppala, S. M., Simmons, A. J., Berrisford, P., Poli, P. and co-authors. 2011. The era-interim reanalysis: configuration and performance of the data assimilation system. *Q. J. Roy. Meteorol. Soc*. **137**(656), 553–597.

DiBattista, M. T. and Polvani, L. M. 1998. Barotropic vortex pairs on a rotating sphere. *J. Fluid Mech*. **358**, 107–133.

Dritschel, D. G. 1985. The stability and energetics of corotating uniform vortices. *J. Fluid Mech*. **157**, 95–134.

Egger, J. 1992. Point vortices in a low-order model of barotropic flow on the sphere. *Q. J. Roy. Meteorol. Soc*. **118**(505), 533–552.

ERA. 2009. *European Centre for Medium-Range Weather Forecasts (ECMWF) Re-Analysis Interim (Era-Interim) Model Data*. NCAS British Atmospheric Data Centre, Oxford.

Friedlander, S. 1975. Interaction of vortices in a fluid on the surface of a rotating sphere. *Tellus*. **27**(1), 15–24.

Friedrich, K. and Bissolini, P. 2011. Die hitzewelle in osteuropa 2011. *Promet*. **27**(1, 2), 44–52.

Garriott, E. B. 1904. Long range forecasts. *U S Weather Bur. Bull*. **35**, 89 pp.

Gröbli, W. 1877. *Specielle Probleme über die Bewegung geradliniger paralleler Wirbelfäden*. Zürcher und Furrer, Zürich.

Helmholtz, H. 1858. Über integrale hydrodynamischer gleichungen welche den wirbelbewegungen entsprechen. *J. Reine Angew. Math*. **5**, 25–55.

Holton, J. R. and Tan, H.-C. 1980. The influence of the equatorial quasi-biennial oscillation on the global circulation at 50 mb. *J. Atmos. Sci.* **37**(10), 2200–2208.

Holton, J. R. and Tan, H.-C. 1982. The quasi-biennial oscillation in the northern hemisphere lower stratosphere. *Meteorol. Soc. Jpn. J.* **60**, 140–148.

Kanamitsu, M., Ebisuzaki, W., Woollen, J., Yang, S.-K., Hnilo, J. J. and co-authors. 2002. NCEP-DOE AMIP-II reanalysis (R-2). *Bull. Am. Meteorol. Soc.* **83**(11), 1631–1643.

Kirchhoff, G. 1876. *Vorlesungen über mathematische Physik I*, Volume 1. Teubner, Leipzig.

Kolmogorov, A. N. 1941. The local structure of turbulence in incompressible viscous fluid for very large Reynolds numbers. *Dokl. Akad. Nauk SSSR.* **30**, 299–303.

Kuhlbrodt, T. and Névir, P. 2000. Low-order point vortex models of atmospheric blocking. *Meteorol. Atmos. Phys.* **73**(3–4), 127–138.

Lim, C., Montaldi, J. and Roberts, M. 2001. Relative equilibria of point vortices on the sphere. *Physica D.* **148**(1), 97–135.

Mayer, A. M. 1878. Floating magnets. *Nature.* **18**, 258–260.

Morikawa, G. K. and Swenson, E. V. 1971. Interacting motion of rectilinear geostrophic vortices. *Phys. Fluids.* **14**(6), 1058–1073.

Müller, A. and Névir, P. 2014. A geometric application of Nambu mechanics: the motion of three point vortices in the plane. *J. Phys. A. Math. Theor.* **47**(10), 105201.

Namias, J. 1947. *Extended Forecasting by Mean Circulation Methods.* Cornell University, US weather bureau, Washington.

NCEP. 2000. *National Centers for Environmental Prediction/ National Weather Service/NOAA/U.S. Department of Commerce, NCEP/DOE Reanalysis 2 (R2). Research Data Archive at the National Center for Atmospheric Research, Computational and Information Systems Laboratory*. NCEP, Silver Spring.

Névir, P. 1998. *Die Nambu-Felddarstellungen der Hydro-Thermodynamik und ihre Bedeutung für die dynamische Meteorologie*. Habilitation dissertation, Free University of Berlin, Berlin.

Newton, P. K. 2013. *The N-Vortex Problem: Analytical Techniques*. Volume 145. Springer Science & Business Media, New York.

NMI. 2014. Norsk riksringkasting. Norwegian Meteorological Institute, Online at: http://artikkel.yr.no/varmeste-juli-pa-over-100-ar-1.11862568

Novikov, E. A. 1975. Dynamics and statistics of a system of vortices. *Zh. Eksp. Teor. Fiz.* **68**, 1868–1882.

Obukhov, A. M., Kurgansky, M. V. and Tatarskaya, M. S. 1984. Dynamic conditions for the origin of drought and other large-scale weather anomalies (Russian). *Meteorol. Hydrol.* **10**, 5–13.

Pelly, J. L. and Hoskins, B. J. 2003. A new perspective on blocking. *J. Atmos. Sci.* **60**(5), 743–755.

Polvani, L. M. and Dritschel, D. G. 1993. Wave and vortex dynamics on the surface of a sphere. *J. Fluid Mech.* **255**, 35–64.

Rex, D. F. 1950a. Blocking action in the middle troposphere and its effect upon regional climate I. *Tellus.* **2**(3), 196–211.

Rex, D. F. 1950b. Blocking action in the middle troposphere and its effect upon regional climate II. *Tellus.* **2**(4), 275–301.

Rex, D. F. 1951. The effect of Atlantic blocking action upon European climate. *Tellus A.* **3**(2), 100–112.

Schielicke, L., Névir, P. and Ulbrich, U. 2015. Kinematic vorticity number – a tool for estimating vortex sizes and circulations. *Tellus A.* (MS ***** - not yet published).

Synge, J. L. 1949. On the motion of three vortices. *Can. J. Math.* **1**(3), 257–270.

Thomson, J. J. 1883. *A Treatise on the Motion of Vortex Rings: An Essay to Which the Adams Prize Was Adjudged in 1882, in the University of Cambridge*. Macmillan, London.

Truesdell, C. 1953. Two measures of vorticity. *Indiana Univ. Math. J.* **2**, 173–217.

Watson, P. A. G. and Gray, L. J. 2014. How does the quasi-biennial oscillation affect the stratospheric polar vortex? *J. Atmos. Sci.* **71**(1), 391–409.

Yeh, T.-C. 1949. On energy dispersion in the atmosphere. *J. Meteorol.* **6**(1), 1–16.